THERMOGRAPHIC INVESTIGATION OF 3.2 mm DIAMETER ORIFICED HOLLOW CATHODES

Matthew T. Domonkos* and Alec D. Gallimore†
Plasmadynamics and Electric Propulsion Laboratory (PEPL)
The University of Michigan
Ann Arbor, MI 48109

Michael J. Patterson‡
NASA Lewis Research Center
Cleveland, OH 44135

Abstract

In an effort to support the needs of emerging low-power electric propulsion systems, efficient, low-current hollow cathodes are being developed at the NASA Lewis Research Center. A thermal model of the hollow cathode is currently under development, and a laboratory model cathode assembly with a removable enclosed keeper was constructed to measure cathode temperature distributions for code validation. The discharge voltage of the cathode was characterized both with the enclosed keeper and in an open geometry with a disk anode. The enclosed keeper configuration exhibited lower voltage operation with higher cathode temperatures over the entire range of operating conditions. In conjunction with the performance evaluations, an imaging radiometer connected to an image acquisition software package was used to measure the cathode temperature distributions along the tube. Thermocouples placed on the cathode were used to calibrate the radiometer. The temperature distributions exhibited complex profiles which indicated either non-uniform emittances or unexpected heat sources. Cathode tube temperature distributions were weakly proportional to flow rate. The temperature distributions along the enclosed keeper also exhibited complex structure. The keeper temperature scaled inversely with the flow rate.

Nomenclature

$p(x)$ = pixel value at x
p_{max}, p_{min} = pixel maximum/minimum value
$T(x)$ = temperature at x (°C)
T_{max}, T_{min} = temperature maximum/minimum (°C)
x = pixel location (mm)
τ = transmittance

Introduction

As part of an ongoing effort at the NASA Lewis Research Center to develop low-power and flow rate cathodes for sub-kilowatt class ion and Hall thrusters and more efficient plasma contactors, a thermographic investigation of 3.2 mm diameter orificed hollow cathodes has been performed.[1,2,3] Scaling of ion and Hall thrusters for low power is more optimal than throttling of kilowatt-class devices to sub-kilowatt powers.[3] To achieve similarity with kilowatt-class ion thrusters, the neutralizer power consumption target for the NASA Lewis 8 cm ion thruster has been set at 2 W.[3] In order to achieve this goal, a cathode model is currently under development to facilitate scaling to low power. Considering that devices reported in the literature[3] require 7 W or greater, an accurate model must address not only the plasma physics and plasma-wall interactions, but also the mechanical complexity and the thermal environment. The complex geometry and composition of hollow cathodes have previously been neglected in the development of cathode energy balances, principally due to the assumption of high power density at currents of 10 A or greater.[4] In order to consider the components of the energy balance previously omitted and the complex geometry of the hollow cathode, the heat transfer code SINDA will be incorporated into the overall cathode model. SINDA has been used with the Thermal Radiation Analysis SYStem (TRASYS) to model the thermal environment of the ion thruster.[5] While codes such as SINDA and TRASYS offer the capability of treating complex geometries, detailed, device-representative temperature maps are needed for code

* Graduate Student Researcher, Student Member AIAA
† Associate Professor, Senior Member AIAA
‡ Research Engineer, Member AIAA

validation. This paper describes the results of an experimental investigation aimed at generating a hollow cathode temperature database by using an imaging radiometer to measure the external cathode temperature distribution.

Most thermal data collected to date has consisted of point measurements from thermocouples or optical pyrometers.[6,7,8,9,10,11] Mirtich and Kerslake[9] used Type R thermocouples to measure both cathode tube and insert temperatures on mercury hollow cathodes. From these data, a rough profile of the temperature distribution along the tube was reported.[9] Experiments performed at Giessen University on enclosed keeper neutralizers included point temperature measurements using a pyrometer, thermocouples, and thermistors.[10,11] In 1979, Seigfried and Wilbur[8] reported on experiments conducted with a quartz tube hollow cathode. This arrangement provided optical access to the insert, and the temperature was measured using a pyrometer.[8] More recently, Salhi[6] measured external cathode temperatures using thermocouples and a pyrometer. Internal insert temperatures were evaluated with a calibrated photodiode connected to the interrogation point by a quartz tube.[6] Thermocouple and pyrometer data were also incorporated into the recent 28,000 hour hollow cathode life test at the NASA Lewis Research Center.[7] All these efforts yielded temperature data at a small number of points.

Thermal imaging offers the potential for non-intrusive resolution of small scale temperature gradients in a hollow cathode assembly. Resolution of small fluctuations is required to validate the thermal modeling of low current hollow cathodes. The purpose of this paper is to present a database of temperature profiles recently obtained over a range of discharge currents and flow rates.

Experimental Apparatus

Cathodes

Since the overall goal of the program reported on here was to develop very-low-power hollow cathodes, some modifications to the cathode assemblies currently in use were employed.[12] Figure 1 illustrates the enclosed keeper geometry. The cathode tube length was extended relative to the other small cathode assemblies to reduce conduction losses, and an enclosed keeper was used to limit the radiation power loss from the cathode tube.[12] The assembly permitted removal of the keeper so that the performance benefits of an enclosed keeper system could be quantified. Figure 2 depicts the open keeper configuration. In this case, a plate keeper with an orifice identical to that in the enclosed keeper was used. The cathode assembly procedure was similar to that detailed elsewhere.[12,13] In addition, a second cathode, designated SC9 (AR3 in Reference 12), with an open keeper configuration was also tested. Performance and fabrication details appear in Reference 12.

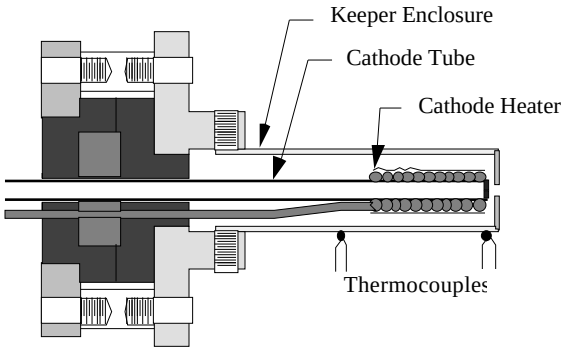

a) Schematic

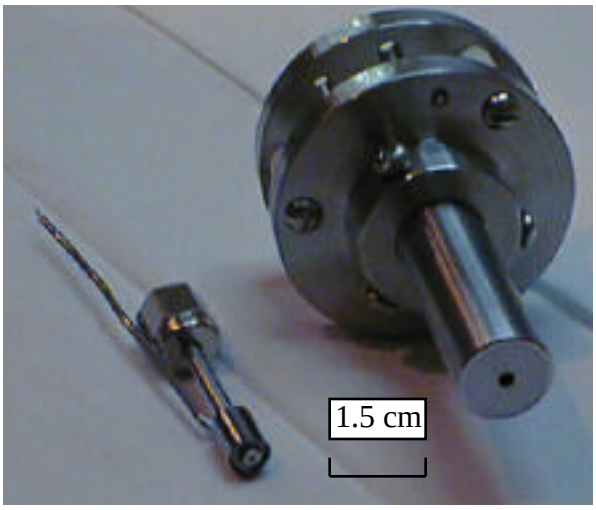

b) Photograph with Cathode and Heater

Figure 1 - The Enclosed Keeper Assembly

Electrical Scheme

The cathode heater was powered by a 16 V, 10 A DC power supply, and a 55 V, 3 A supply maintained the discharge, as shown in Figure 3. The supplies were controlled by a computer based data acquisition and control system. Discharge current and voltage data were stored at regular intervals, and control limits were programmed to shutdown the cathode in the event of a harmful operating condition. In addition, an oscilloscope was used to monitor the discharge current and voltage on short time scales where the

noise inherent to plume mode onset. A plume mode discharge is characterized by high frequency and large amplitude voltage oscillations, and is induced by a reduction in flow rate until the anode (keeper) sheath extends to the cathode. In addition to the current and voltage, the data acquisition program was configured to read the chamber pressure, several thermocouple outputs, the output of an optical thermometer reading the orifice plate temperature, and the cathode mass flow rate.

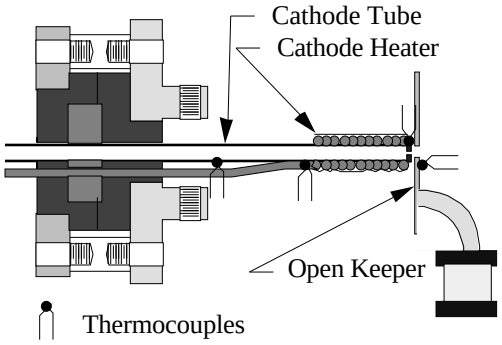

a) Schematic

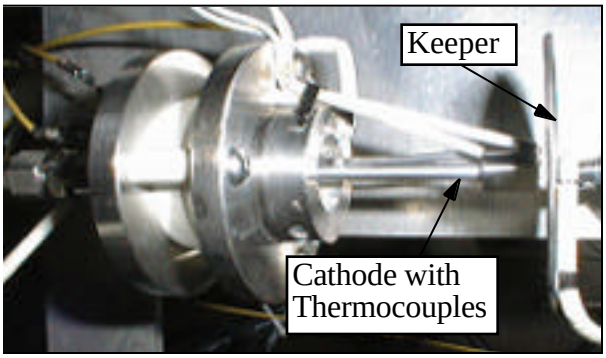

b) Photograph with Thermocouples
Figure 2 - The Open Keeper Assembly

Propellant Feed System

Research grade xenon (99.999%) was supplied to the cathode via the expellant feed system illustrated in Figure 4. Electropolished stainless steel tubing 6.4 mm in outer diameter was used with ultra-high vacuum metal gasket seals at all junctions. A capacitance manometer was used to quantify the leak rate after alterations to the feed system. The flow rate was calibrated using a bubble flow meter over the range from 0.5 to 5 sccm, and the error in the flow rate measurement was approximately constant at ±0.06 sccm over the range of flow. The delivery pressure of the regulator was set to 253 kPa (22 psig), and the flow rate was controlled using a mass flow controller. The feed system is equipped with an in-line calibrator which enables flow rate calibration during operation.

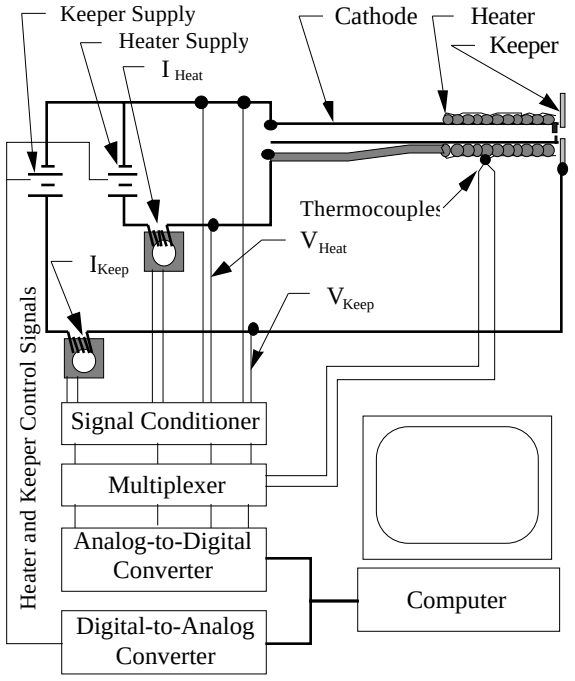

Figure 3 - VF-52 Diagnostics and Control System

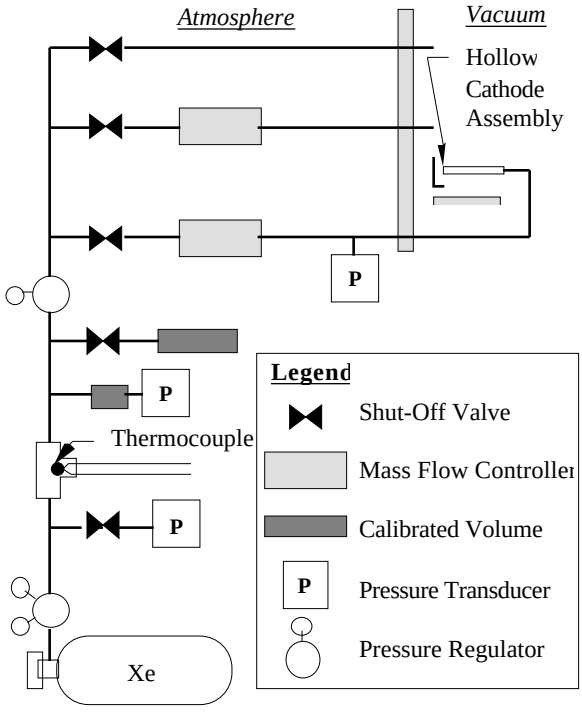

Figure 4 - VF-52 Flow System Schematic

Vacuum Facility 52

The tests reported here were conducted in Vacuum Facility 52 (VF-52), shown in Figure 5, at the NASA Lewis Research Center. VF-52 is a 61 cm diameter by 90 cm long chamber. A 25 cm diameter cryogenic vacuum pump was used to maintain a high vacuum in the chamber. The pump speed on Xe was approximately 1050 L/s, and operating pressures ranged from 2.7×10^{-3} to 5.3×10^{-3} Pa. The pressure was measured using a Bayard-Alpert ion gage.

Figure 5 - The VF-52 Test Stand at the NASA Lewis Research Center

Cathode Performance

Cathode operation and performance evaluations were conducted similarly to those reported in Reference 12. The cathodes were run initially for approximately two hours before the performance characterization was initiated. The flow rate was changed at constant currents of 0.75, 1.00, and 1.50 A. The results of the performance characterization of both the enclosed and open keeper configurations are presented in Figure 6. The enclosed keeper geometry operated at lower voltage for all current and flow rate combinations and showed a smaller variation of discharge voltage with flow rate. Both configurations showed a gradual discharge voltage increase until plume mode was induced at low flow rates. At 1.50 A, the cathode remained in spot mode for both configurations over the range of flow rates tested. The open keeper configuration demonstrated anomalous behavior at 1.00 A, although this was likely an anode effect as will be discussed later.

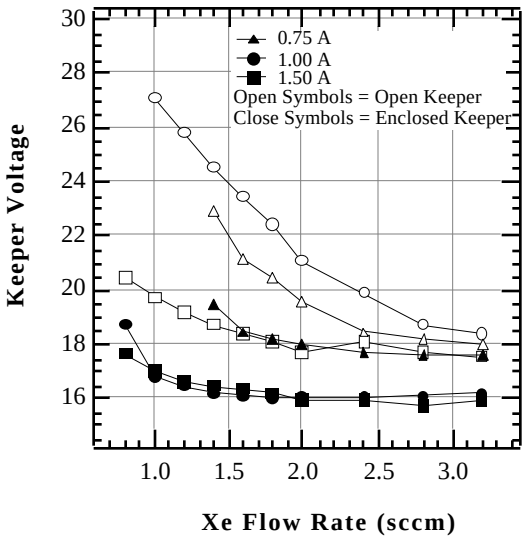

Figure 6 - Performance Characterizations of Both the Enclosed and Open Keeper Assemblies

Thermal Imaging System

Cathode temperature profiles were acquired with the imaging system illustrated in Figure 7. The overall scheme was conceptually similar to that reported by Polk and Goodfellow[14] with appropriate modifications based on the expected temperature range. A commercially available imaging radiometer was used because the anticipated temperature range required the capability of scanning beyond visible wavelengths. The radiometer had a spectral bandpass of 8-12 μm. A coated zinc selenide viewport, with a transmittance greater than 95% between 8 and 12 μm, was installed for these experiments. The radiometer incorporated germanium optics which have a high transmittance in the infrared. A 3.0x germanium telescope, with a transmittance of 0.80, was used to enlarge the cathode image. Within the radiometer, incoming light was scanned horizontally and vertically using electromechanical servos and focused onto a mercury-cadmium-telluride detector. The detector was encased in a dewar cooled by liquid nitrogen. The finite size of the detector limited the true spatial resolution of the diagnostic. This limitation was especially apparent at boundaries where emissivity and temperature changed over a small distance. The effect was to attenuate the measurement in the high intensity region and to inflate the values in the low temperature area. The extent to which this occurred in this investigation will be discussed later. The

system was rated for temperatures ranging from 0 to 1500 °C with selectable spans from 5 to 500 °C. Each of these temperature spans had a maximum dynamic range of 8 bits using the image averager.

The video output of the radiometer was connected to an 8 bit greyscale frame grabber board in a computer. The greyscale acquisition relied only on the luminance portion of the video signal. The resulting image on the computer had an intensity between 0 and 255 dependent upon the input luminance. The radiometer system attached a greyscale bar to the image as seen in Figure 8, which was used as a check of the linearity of the transfer function of the frame grabber board; a linearly increasing profile of the pixel intensity in the greyscale bar ensured that the radiometer output was being represented accurately on the computer. The line profile tool in the image acquisition package was used to evaluate the distribution of pixel intensity along a line drawn on the image. The pixel profile was related to the temperature profile through the transfer functions. For this investigation, only centerline profiles were acquired since the emitted radiation intensity depended only on the normal emittance; this technique minimized variation in the emittance due to geometric effects.

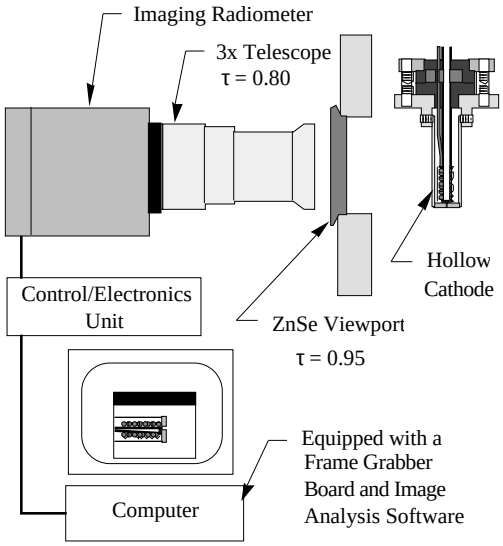

Figure 7 - Thermography Experimental Set-Up

Calibration of the Radiometer

Although the radiometer was capable of correcting for the estimated emittance of the cathode and the transmittances of the viewport and lenses, the images were left uncorrected for the following reasons: 1) uncertainty in the emittance of the target as a function of wavelength and temperature and 2) uncertainty in the true transmittance of the optics. Instead, the temperature profiles were compared with thermocouple data to provide a calibration. This method assumed that the thermocouples were in equilibrium with the cathode tube at the point of interrogation, that they were a negligible heat sink, and the temperature distribution was azimuthally symmetric, since the thermocouples were located opposite of the radiometer. Type R thermocouples were spot welded to selected locations on the cathode and keeper. Although the spot weld provided a low thermal resistance contact between the thermocouple and the cathode or keeper, the tendency of the thermocouple to act as a heat sink was mitigated by using 0.25 mm diameter wire. The assumption of azimuthal symmetry was taken for convenience, and the results of the destructive analysis of the 28,000 hour hollow cathode suggest a high degree of azimuthal symmetry for all the cathode properties.[7] The calibration procedure required at least two thermocouple references on each material in the field of view of the radiometer. With two temperature measurements, a slope and an offset were determined using Equation 1 for the transfer function between pixel luminance and temperature.

$$T(x) = \left(p(x) - p_{\min}\right)\frac{\left(T_{\max} - T_{\min}\right)}{\left(p_{\max} - p_{\min}\right)} + T_{\min} \qquad (1)$$

Essential to an accurate temperature calibration, position calibrations were performed using known references within the image. A scratch was placed in the enclosed keeper approximately 25.4 mm from the exit, and this reference point was visible as seen in Figure 8a-b (lower right quadrant of the keeper). The centerline of the keeper was kept free of marks to minimize alteration of the emitted radiation profile. For the open keeper geometry, the boundaries of the heater shield were used as reference. Figure 8c-d show the shield edges which exhibited similar definition throughout the testing conditions. The position calibration was saved to the computer viewport which provided the same scale for all the images collected during a test. Thermocouples were located roughly in the positions indicated in Figure 1 and 2. In the case of the enclosed keeper, only two thermocouples were required for calibration since the material properties were assumed to be uniform. One thermocouple was located on the side of the keeper within 1 mm of the end, and the other was approximately 26 mm upstream on the same side. The heater shield

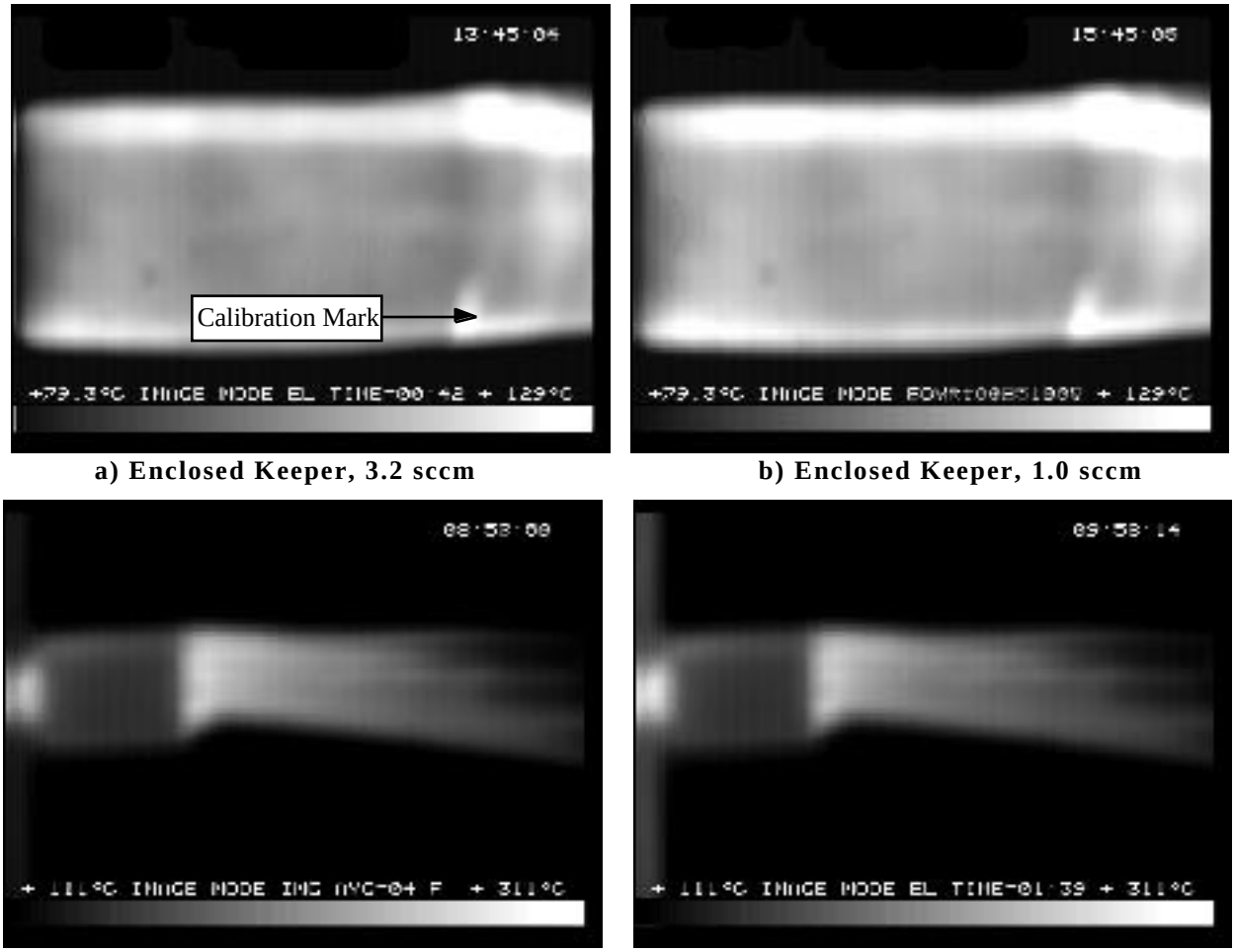

a) Enclosed Keeper, 3.2 sccm **b) Enclosed Keeper, 1.0 sccm**

c) Open Keeper, 3.2 sccm **d) Open Keeper, 1.4 sccm**

Figure 8 - Raw Images from the Radiometer

temperature profile was relatively constant for most of the preliminary tests. Consequently for the open keeper configuration, thermocouples were attached to the cathode tube near the orifice, immediately upstream of the heater, and approximately 26 mm upstream of the heater. These thermocouples enabled temperature profiles to be evaluated along the exposed section of the cathode tube.

Profile Acquisition and Processing

Once the camera was sighted on the cathode or keeper and the spatial calibration was configured, data acquisition consisted of grabbing a frame and downloading the line profile. The frame grabber software was configured to average 10 images, which when combined with the four image average performed by the radiometer control package, yielded an overall averaging of 40 frames. Further averaging appeared to have a negligible impact on the smoothness of the line profiles. Images were acquired at all the conditions represented in the performance characterization (Figure 6). Temperatures and operating conditions were recorded for reference and calibration of the image data.

The line profile data were recorded as a spreadsheet column. From the spatial calibration, position in the column was related to a location along the cathode or keeper centerline. Next, the pixel intensity was correlated to the thermocouple measurements. Thus by definition the line profiles matched the thermocouple data reported here. Figure 9 shows a line profile prior to temperature calibration. As mentioned earlier, sharp temperature gradients posed a limitation on the diagnostic, and Figure 9 illustrates the useful portion of the line profile.

Error Analysis of the Temperature Measurements

An assessment of the uncertainty in the temperature profiles must include calibration, random, and systematic errors. The thermocouple readout was calibrated against a National Institute of Standards and Technology (NIST) traceable standard prior to the tests reported here. The ANSI tolerances for type R

thermocouples are ±1.4 °C from 0 to 538 °C and ±0.25 percent from 538 to 1482 °C.[15] Random errors in the thermocouple measurements were negligible since readout values never oscillated more than 0.5 °C during a sampling. The systematic errors in the calibration were discussed previously. In the worst case for the thermocouple attached to the orifice plate, the power conducted away from the site was on the order of 1000 times smaller than the discharge power and comparable to the radiative component in the absence of the thermocouple.[16] Consequently the calibration standard had an estimated uncertainty of less than 1 percent.

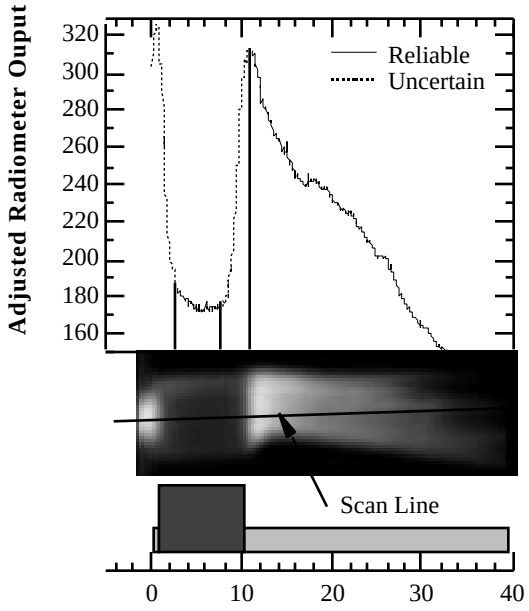

Figure 9 - Sample Data From Radiometer

Random fluctuations of the image data were minimized by averaging 40 frames for each measurement. Still as can be seen in Figure 9, a significant amount of scatter appeared in the line profiles. By averaging the data in the vicinity of each pixel, a relatively scatter-free profile was obtained. This technique was employed for the data reported here, resulting in a negligible random error.

Calibrating the image against thermocouple data eliminated the difficulty in obtaining a thorough characterization of the surfaces and optics which would be required to treat the radiometer output as an absolute measurement of the two-dimensional temperature field. The largest source of systematic error was associated with the inability of the radiometer to handle large temperature gradients in the two-dimensional space of the image. This effect can be seen most clearly in Figure 8a-b. The keeper tube received radiated energy from the cathode and heat conducted away from the keeper orifice. Consequently, it was expected that the downstream end of the keeper would have the highest temperature with the radiation from the cathode a smaller contributor along the axis. The images indicated a sharp temperature decrease toward the downstream end. Consequently this portion of the profile was not used. Immediately upstream of the fall-off, the profile indicated an approximately linear increase in temperature toward the downstream end. Since the profile data near the downstream end of the tube were considered inaccurate, and one of the thermocouples used for calibration was located beyond the limits of the accurate data, a line fit, based on the slope of the downstream data, was used to extrapolate the profile to the calibration point. A similar method was adopted with the open keeper configuration because the thermocouple at the base of the cathode was outside of the field of view of the radiometer. The extrapolation occurred over a distance of approximately 4 mm for the open keeper configuration and 6 mm for the enclosed keeper. In both cases, the conditions across the extrapolation were expected vary gently. The span of thermocouple derived keeper temperature data (typically only about 30 °C) supports this expectation. Consequently, the uncertainty introduced by this method was expected to be small.

In conclusion, the calibration errors were found to be approximately one percent. Random errors in the radiometer system were negligible. Although systematic errors were potentially large, the extrapolation of the profiles was expected to yield only small uncertainties in the profiles.

Thermography Results

As stated previously, infrared images of the cathode assemblies were acquired at each of the conditions tested in the performance evaluation (see Figure 6). Representative data of the cathode tube temperature profiles is presented in Figure 10. The axial position has been adjusted for the benefit of the reader; zero indicates the exit plane of the cathode. The profiles presented are at a mass flow of 2.4 sccm and the flow rate where the transition to plume mode occurred. The profiles varied slowly as a function of flow rate. Thermocouple data are included for reference.

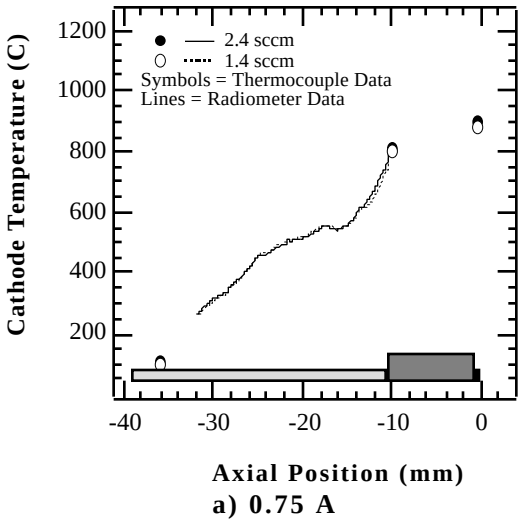

a) 0.75 A

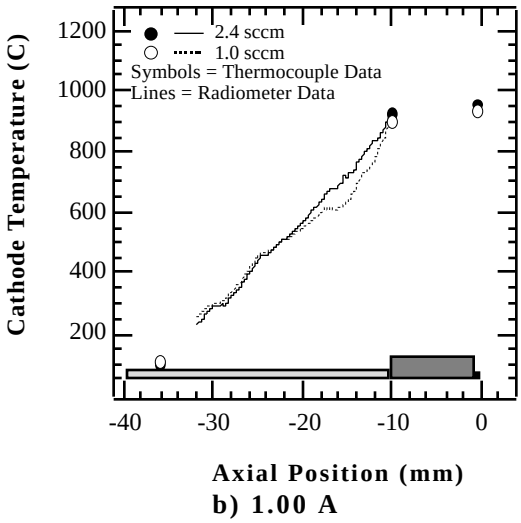

b) 1.00 A

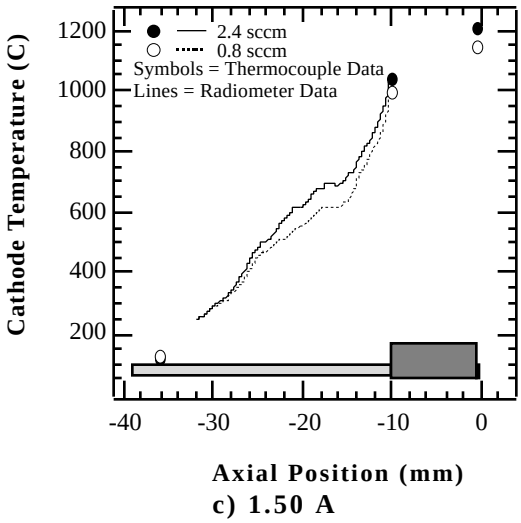

c) 1.50 A

Figure 10 - Tube Temperature Profiles for the Open Keeper Assembly in Spot (2.4 sccm) and Plume Modes

Figure 10a depicts the tube temperature profile for the open keeper geometry at 0.75 A. At -11 mm, the profile initially drops away sharply with distance from the orifice, and the slope gradually decreases in magnitude. The curvature gives an indication of the relative power losses due to radiative and conduction losses. A slight bump appears in the profile at approximately -18 mm. As will be discussed later, this appears to be a device-specific phenomenon. As seen in Figure 10b, the bump is absent from the profile at 2.4 sccm, which was the first data taken with the open keeper configuration. The phenomenon set in within two hours as indicated by the qualitative difference in profiles for 1.0 and 2.4 sccm. In all cases, the temperature profiles were undifferentiated with flow rate beyond 30 mm upstream of the orifice. The profiles at 1.00 and 1.50 A also show a significant difference between spot and plume modes. Although the attachment region on the insert extends upstream with decreasing flow rate,[8] the tube temperature was observed to scale with the flow rate. This will be discussed in terms of the anode (keeper) power deposition. Figure 11 depicts a comparison between the open-keeper assembly cathode and a geometrically similar cathode, designated SC9 here (AR3 in Reference 12), with a shorter tube and orifice length. The tube temperature decayed monotonically with distance from the orifice plate, indicating that the phenomenon observed with the open-keeper cathode was device-specific. The long tube employed with the open keeper also served the designed purpose of facilitating high temperature operation.

In addition to axial temperature profiles, orifice plate temperature data were collected with an optical thermometer. These data are presented in Figure 12. The anomalous behavior of the open keeper cathode at 1.00 A was again evident with the orifice plate operating as cool at 1.00 A as at 0.75 A; the enclosed keeper cathode exhibited more than a 50 °C decrease for the same change in current. Considering that the power consumption at 1.00 A was far greater than that at 0.75 A for the open keeper and the low operating temperature of the cathode, the input power must have been deposited to the keeper.

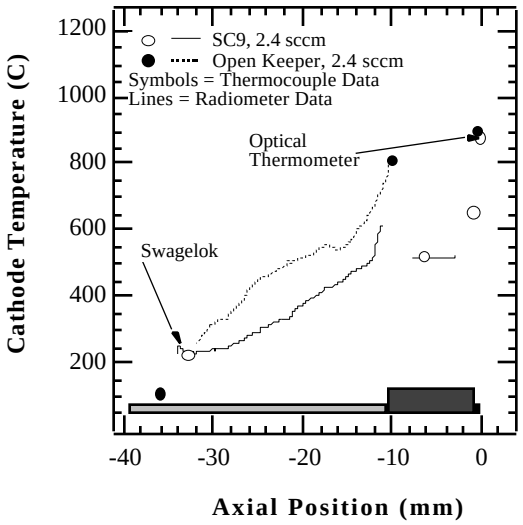

Figure 11 - Temperature Profile Comparison with SC9 (AR3) at 0.75 A and 2.4 sccm.

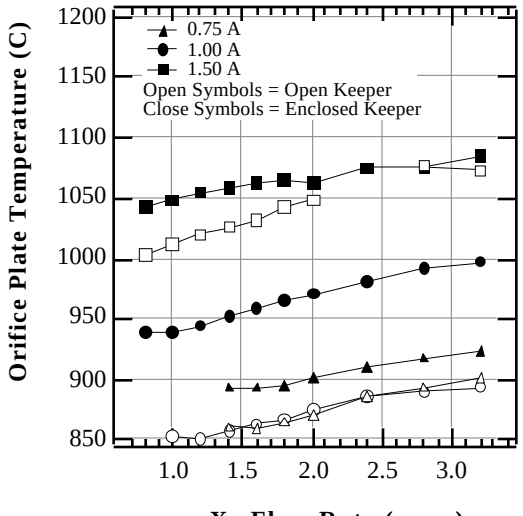

Figure 12 - Orifice Plate Temperatures Measured with the Optical Thermometer

The temperature data, shown in Figure 13, for the keeper in the open configuration support the conclusion that most of the anomalously large input power at 1.00 A was deposited in the anode. The keeper temperature increased monotonically with decreasing flow. At 1.00 A, the keeper temperature was comparable to that at 1.50 A. The general trends seen in Figure 13 were also present in the temperature profile data shown in Figure 14 for the enclosed keeper assembly. The onset of plume mode created a large increase in the mean temperature along the profile. The shape between -7 and -27 mm appears to reflect radiative heat transfer from the cathode tube; the drop around 12 to 16 mm roughly corresponds to the location of the cathode heater shields which radiate considerably less than the cathode tube (Figure 11). The increase in keeper temperature beyond -27 mm was also seen in the raw images shown in Figure 8.

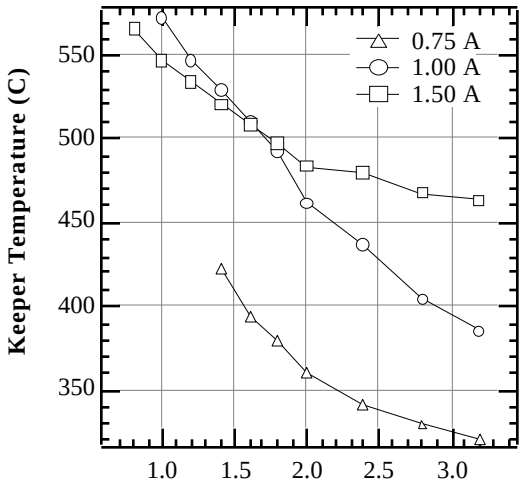

Figure 13 - Keeper Temperature Variation for the Open Geometry Cathode

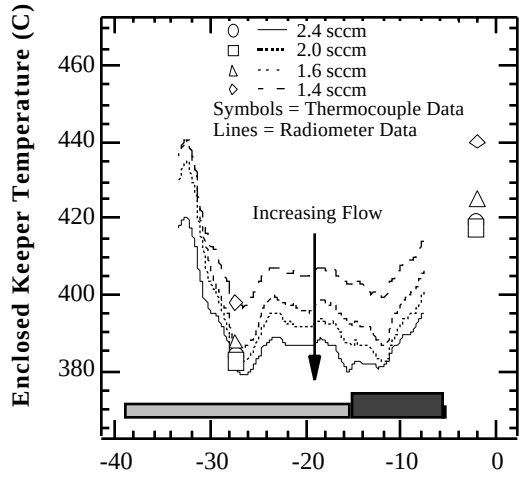

Figure 14 - Variation of Enclosed Keeper Temperature Profiles at 0.75 A.

Conclusions

Examination of the enclosed keeper geometry was aimed at quantifying the benefits of this configuration for cathode performance and lifetime. Performance characterizations indicated that the enclosed keeper assembly operated more efficiently over the range of operating conditions. The discharge voltage was also relatively insensitive to flow rate except near the

threshold for the transition from spot to plume mode. Temperature profiles for the cathode tube exhibited a complex structure which appeared to be a device-specific condition that developed over the course of several hours of operation. The temperature distribution along the enclosed keeper also exhibited a high degree of complexity, the nature of which was not full understood. The variation of keeper temperatures indicated an inverse relationship with mass flow rate and a strong proportionality with the current.

The results obtained with the imaging radiometer to date have been somewhat limited by the calibration method and the assumption of uniform emittance over a large temperature range. Refinement of the diagnostic would enable a determination of the surface emittance and reduce the uncertainty associated with the high temperature gradient regions. In addition, cutting optical ports in the enclosed keeper would enable cathode tube temperature measurements without significantly altering the environment created by the enclosed keeper. Both of these modifications to the diagnostic are the subject of future work.

Acknowledgments

This work was performed at the NASA Lewis Research Center under Grant No. NGT-3-52311. The authors greatly appreciate the invaluable assistance provided by Michael Pastel, Ralph Jacko, Robert Roman, Timothy Sarver-Verhey, and George Soulas.

References

[1] Patterson, M. J. and Oleson, S. R., "Low Power Ion Propulsion for Small Spacecraft," AIAA Paper No. 97-3060, *33rd AIAA Joint Propulsion Conference*, Seattle, WA, July, 1997.

[2] Patterson, M. J., Verhey, T. R., Soulas, G., and Zakany, J., "Space Station Cathode Design, Performance, and Operating Specifications," IEPC Paper No. 97-170, *25th International Electric Propulsion Conference*, Cleveland, OH, Aug. 1997.

[3] Patterson, M. J., Grisnik, S. P., and Soulas, G. C., "Scaling of Ion Thrusters to Low Power," IEPC Paper No. 97-098, *25th International Electric Propulsion Conference*, Cleveland, OH, Aug. 1997.

[4] Siegfried, D. E. and Wilbur, P. J., "A Model for Mercury Orificed Hollow Cathodes: Theory and Experiment," *AIAA Journal*, Vol. 22, No. 10, Oct. 1984, pp. 1405-1412.

[5] Van Noord, J., Gallimore, A., and Rawlin, V., "Numerical Thermal Model of a 30-cm NSTAR Ion Thruster," IEPC Paper No. 97-185, *25th International Electric Propulsion Conference*, Cleveland, OH, Aug. 1997.

[6] Salhi, A., *Theoretical and Experimental Studies of Orificed, Hollow Cathode Operation*, Ph. D. Dissertation, 1993.

[7] Sarver-Verhey, T. R., "28,000 Hour Xenon Hollow Cathode Life Test Results," IEPC Paper 97-168, *25th International Electric Propulsion Conference*, Cleveland, OH, Aug. 1997.

[8] Seigfried, D. E. and Wilbur, P. J., "Studies on an Experimental Quartz Tube Hollow Cathode," AIAA Paper No. 79-2056, *Princeton/AIAA/DGLR 14th International Electric Propulsion Conference*, Princeton, N.J., Oct.-Nov., 1979.

[9] Mirtich, M. J. and Kerslake, W. R., "Long Lifetime Hollow Cathodes for 30-cm Mercury Ion Thrusters," AIAA Paper No. 76-985, *AIAA International Electric Propulsion Conference*, Key Biscayne, FL, Nov. 1976.

[10] Groh, K. H., Walther, S. E., and Loeb, H. W., "Recent Neutralizer Investigations at Giessen University," AIAA Paper No. 76-989, *AIAA International Electric Propulsion Conference*, Key Biscayne, FL, Nov. 1976.

[11] Walther, S. E., Groh, K. H., and Loeb, H. W., "Experimental and Theoretical Investigations of the Giessen Neutralizer System," AIAA Paper No. 78-706, *AIAA/DGLR 13th International Electric Propulsion Conference*, San Diego, CA, Apr. 1978.

[12] Domonkos, M. T., Gallimore, A. D., and Patterson, M. J., "Parametric Investigation of Orifice Aspect-Ratio on Low Current Hollow Cathode Power Consumption," AIAA Paper No. 98-3345, *34th AIAA Joint Propulsion Conference*, Cleveland, OH, July 1998.

[13] Sarver-Verhey, T. R., "Extended Test of a Xenon Hollow Cathode for a Space Plasma Contactor," NASA Contractor Report 195402, Nov. 1994.

[14] Polk, J. E. and Goodfellow, K. D., "High Current Cathode Thermal Behavior, Part II: Experiments," IEPC Paper No. 93-029, *Proceedings of the 23rd International Electric Propulsion Conference*, Seattle, WA, Sept. 1993, pp. 293-303.

[15] McGee, T. D., *Principles and Methods of Temperature Measurement*, John Wiley & Sons, Inc., New York, 1988.

[16] Yaws, S. L., *Handbook of Thermal Conductivity, Volume 4: Inorganic Compounds and Elements*, Gulf Publishing Company, Houston, TX, 1997.